Liquid Crystals
Publication details, including instructions for authors and subscription information:
http://www.informaworld.com/smpp/title~content=t713926090

Molecular segregation and aggregate shape in a lyotropic rectangular phase

Stefan Gustafsson[a]; Per-Ola Quist[a]; Bertil Halle[a]
[a] Condensed Matter Magnetic Resonance Group, Chemical Center, Lund University, Lund, Sweden

To cite this Article Gustafsson, Stefan , Quist, Per-Ola and Halle, Bertil(1995) 'Molecular segregation and aggregate shape in a lyotropic rectangular phase', Liquid Crystals, 18: 4, 545 — 553
To link to this Article: DOI: 10.1080/02678299508036657
URL: http://dx.doi.org/10.1080/02678299508036657

LIQUID CRYSTALS, 1995, VOL. 18, NO. 4, 545–553

Molecular segregation and aggregate shape in a lyotropic rectangular phase

by STEFAN GUSTAFSSON*, PER-OLA QUIST, and BERTIL HALLE

Condensed Matter Magnetic Resonance Group, Chemical Center,
Lund University, P.O. Box 124, S-22100 Lund, Sweden

(*Received 15 April 1994; in final form 15 August 1994; accepted 25 August 1994*)

The microstructure of the rectangular phase in the system sodium decylsulphate/decanol/water is investigated by means of deuterium NMR. By analysing the lineshape from selectively deuteriated decylsulphate and decanol, we separate the effects of (i) the shape anisotropy of the aggregate cross-section and (ii) the inhomogeneous distribution of the two surfactants within the aggregate. The aspect ratio of the cross-section is determined to $1{\cdot}39 \pm 0{\cdot}01$, substantially smaller than previous estimates. We find no evidence for anisotropic growth of the aggregate cross-section in the hexagonal phase, as previously suggested. Rather, the aggregate shape appears to change abruptly at the hexagonal–rectangular phase transition with little change (with temperature) thereafter. The distribution of decylsulphate and decanol within the aggregates of the rectangular phase is highly non-uniform; the decanol concentration is 3 times higher in the central lamellar region than in the curved edges, while the decylsulphate accumulates in the curved regions. This molecular segregation can be rationalized in terms of electrostatic interactions within and between the aggregates.

1. Introduction

Many binary and ternary surfactant–water systems exhibit, besides the classical hexagonal (H_α) and lamellar (L_α) liquid crystal phases, one or two phases with two-dimensional rectangular lattice symmetry [1–3]. Such rectangular (R_α) phases, usually occurring at compositions intermediate between those of the H_α and L_α phases, have been shown to consist of rod-like surfactant aggregates of non-circular cross-section, arranged on a primitive (plane group pmm or pgg) or centred (plane group cmm) two-dimensional rectangular lattice.

In contrast to the classical spherical, cylindrical, and lamellar microstructures (as well as bicontinuous microstructures built from minimal surfaces), the microstructure in the R_α phase exhibits an inhomogeneous interfacial mean curvature. This implies that the surfactant head group area varies over the aggregate surface and, in mixed surfactant aggregates, that the two components are inhomogeneously distributed within the aggregate. Such molecular segregation may play an important role in stabilizing the R_α phase.

The ternary system sodium decylsulphate (SdS)/decanol/water, extensively studied by Hendrikx, Charvolin, and co-workers [4–7], has been reported to exhibit two R_α phases. From the lattice parameters, determined by X-ray scattering, the area of the aggregate section is obtained. If the smallest aggregate dimension can be estimated, the anisometry (aspect ratio) of the cross-section can thus be determined [4]. Neutron scattering techniques have also been used to determine the dimensions of the aggregate cross-section [6] and to obtain *qualitative* evidence of molecular segregation [5].

Here we report the results of an NMR lineshape study of one of the R_α phases in the system SdS/decanol/water. By analysing the quadrupolar lineshapes from the α-deuterons in *both* surfactants, we can accurately determine the aspect ratio of the cross-section as well as quantitatively characterize the spatial variation of the local concentration and orientational order of SdS and decanol within the aggregate. The deuterium NMR approach for studying microstructure in R_α phases was pioneered by Chidichimo, Doane, and co-workers [8–11] and has subsequently been developed and applied by others [12–18]. In a study similar to the present one, Pope and Doane [11] determined the aggregate geometry and molecular segregation in the R_α phase of the ternary system potassium palmitate/benzyl alcohol/water. To our knowledge, however, this is the first *quantitative* study of molecular segregation in an ionic liquid crystal phase, where the inhomogeneous surface charge density is coupled to the electrostatic interactions between the aggregates.

* Author for correspondence.

0267–8292/95 $10·00

2. Experimental

2.1. *Materials and sample preparation*

The samples were made by weighing SdS (sodium decylsulphate), *n*-decanol, and water into glass tubes, which immediately were flame-sealed. The samples were vigorously mixed once a day during three weeks and then equilibrated for another five weeks prior to the measurements. During the equilibration period, the samples were stored at 22 ± 2°C. Because of the limited extension of the R_α phase (cf. below and figure 1), the equilibration procedure is critical.

Samples of three different isotopic compositions were prepared: (i) for phase diagram studies, we used ordinary SdS (> 99 per cent, E. Merck or > 99 per cent, Heraus), *n*-decanol (specially pure, Merck Ltd) and a mixture of ordinary water (doubly distilled) and D_2O (> 99 per cent, Sigma); (ii) sample **S** with α-deuteriated SdS (Synthelec), ordinary *n*-decanol and ^2H-depleated H_2O (Sigma); (iii) sample **D** with α-deuteriated *n*-decanol (> 99 per cent, Larodan), ordinary SdS and ^2H-depleted H_2O. The phase boundaries were found to be independent of the isotopic composition as long as the molar composition was the same.

Samples **S** and **D**, which were used to investigate molecular segregation and aggregate shape in the R_α phase, had a composition SdS/decanol/water of 7·05/1·50/91·45 mol %. The R_α phase obtained at this composition was stable in the range 20–30°C. Above 35°C the sample was in a two-phase region with the H_α phase in equilibrium with a small amount of L_α phase.

2.2. *NMR experiments*

The ^2H NMR experiments were performed on two NMR spectrometers: a Varian Unity 300 equipped with a 10 mm vertical saddle-coil probe and a 7·05 T superconducting magnet and a Bruker MSL 100 equipped with either (*a*) a 10 mm vertical saddle-coil probe and a 2·35 T superconducting magnet, or (*b*) a 10 mm vertical solenoid-coil probe and a Drusch electromagnet (EAR 35N) with the horizontal field locked at 2·00 T. In the latter configuration, the sample tube was connected to a step motor (1600 steps/revolution) allowing angular dependent studies.

The ^2H spectra were accumulated with the standard quadrupolar echo sequence $(90)_x$–τ–$(90)_{\pm y}$–τ–acq., with the delay time $\tau \approx 150\,\mu s$. The 90° pulse duration was approximately 10 μs (Bruker) or 25 μs (Varian). Typically, the spectral width was set to 100–200 kHz and the free induction decay contained 256–512 data points (except for ^2H_2O spectra). Prior to Fourier transformation, the free induction decay was zero-filled to an appropriate level. The temperature was controlled by air-flow regulators, yielding a stability of ± 0·2°C or better.

The acquisition of the ^2H spectra of samples **S** and **D** was performed by increasing the temperature step-wise from 25°C to 50°C. At each temperature the samples were equilibrated for *c.*1 h prior to acquisition.

2.3. *Phase studies*

The relevant region of the phase diagram of the SdS/decanol/D_2O system was mapped at 25°C using *c.*90 samples of different compositions. To distinguish between the different single-phase regions and the intermediate polyphasic regions, we used the ^2H spectrum of D_2O. The single-phase regions were identified from the spectra as follows: a single narrow peak—isotropic phase; two narrow peaks of equal amplitude (or an aligning powder spectrum)— nematic phase; a biaxial powder-like spectrum—R_α phase; a uniaxial powder spectrum with a small (large) splitting—H_α (L_α) phase. For the H_α and L_α phases, the splittings were analysed taking into account the variation of the residual quadrupole coupling constant with composition. The asymmetry parameter of the biaxial D_2O spectra from the R_α phase was in the range 0·9–1·0, with a maximum in the middle of the R_α phase. Spectra from polyphasic samples were identified as superpositions of single-phase spectra. Small fractions of one phase were identified by the spectral singularities of that component ($\theta = 90°$ for uniaxial phases, $\theta = 90°$, $\phi = 0°$ for the

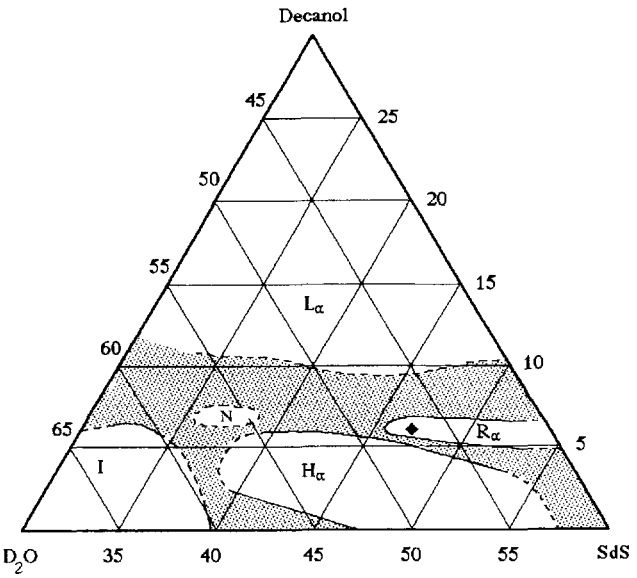

Figure 1. Partial phase diagram (wt %) for the system SdS/decanol/D_2O at 25°C showing the extension of the one-phase regions of the isotropic micellar phase (I) and the hexagonal (H_α),, lamellar (L_α), rectangular (R_α), and nematic (N) liquid crystalline phases. (The dashed phase boundaries have not been accurately determined.) The diamond gives the (isotope corrected) composition of samples **S** and **D**.

biaxial phase, and the narrow peaks in isotropic or nematic phases).

The determined single-phase regions are shown in the partial phase diagram of figure 1. The two-phase regions surrounding the R_α phase have the following approximate extensions: $R_\alpha + H_\alpha$—the shaded region with >43 wt % SdS and $<6{\cdot}5$ wt % decanol; $R_\alpha + L_\alpha$—the shaded region with >52 wt % SdS and $>6{\cdot}5$ wt % decanol.

As compared to a previously published phase diagram [4, 6], figure 1 shows an R_α phase of much smaller extension. The difference in phase behaviour may be ascribed to impurities and to partial hydrolysis of SdS into decanol in previous studies [7]. According to Hendrikx and Charvolin [6, 7], there are two adjacent R_α phases, of symmetries cmm and pgg, in the phase diagram. In view of the different phase behaviour, we cannot say whether our **S** and **D** samples are of cmm or pgg symmetry. Fortunately, however, our conclusions regarding aggregate shape and molecular segregation are virtually independent of the assumed lattice symmetry (cf. § 4.1).

3. Lineshape analysis

3.1. *General considerations*

The normalized spectral line shape for a spin $I = 1$ nucleus in a biaxial phase is given by

$$L(\omega) = \frac{1}{2\pi}\int_0^{2\pi} d\phi \int_0^{\pi} d\theta \sin\theta f(\theta,\phi) \times \left\{\frac{R}{R^2 + [\omega - \omega_Q(\theta,\phi)]^2} + \frac{R}{R^2 + [\omega + \omega_Q(\theta,\phi)]^2}\right\}, \quad (1)$$

with the quadrupolar frequency

$$\omega_Q(\theta,\phi) = \frac{3\pi}{4}\langle\chi\rangle(3\cos^2\theta - 1 + \eta\sin^2\theta\cos 2\phi). \quad (2)$$

Here $f(\theta,\phi)$ is the normalized distribution function for the polar (θ) and azimuthal (ϕ) angles, specifying the orientation of the magnetic field with respect to the principal axes system of the motionally averaged electric field gradient (EFG) tensor. This frame is fixed in the unit cell of the liquid crystal, but its orientation depends on the structure of the surfactant aggregates and on their spatial arrangement within the unit cell (cf. below). In terms of the principal components $\langle V_{xx}^C\rangle$, $\langle V_{yy}^C\rangle$ and $\langle V_{zz}^C\rangle$ of the motionally averaged EFG tensor, one conventionally defines the (motionally averaged) quadrupole coupling constant (QCC), $\langle\chi\rangle$, and asymmetry parameter, η, as

$$\langle\chi\rangle = (eQ/h)\langle V_{zz}^C\rangle, \quad (3)$$

and

$$\eta = [\langle V_{xx}^C\rangle - \langle V_{yy}^C\rangle]/\langle V_{zz}^C\rangle. \quad (4)$$

Finally, R is the transverse relaxation rate. From quadrupolar echo decay experiments on aligned samples, we obtain for the H_α and the R_α phases in the temperature range 25–50°C, $R = 500$–$600\,s^{-1}$ at $\theta = 0°$ and $R = 300$–$350\,s^{-1}$ at $\theta = 90°$. Since R/π is much smaller than $\langle\chi\rangle$, we neglect the orientation dependence of R.

The desired information about the microstructure of the R_α phase is contained in the motionally averaged QCC $\langle\chi\rangle$ and the asymmetry parameter η. To extract these quantities from the observed lineshape $L(\omega)$, we must, in principle, specify the distribution function $f(\theta,\phi)$ for the orientation of the micro-crystallites in the sample. There are two simple limiting cases: a homeotropically aligned sample with $f(\theta,\phi) = \delta(\theta - \theta_0)\delta(\phi - \phi_0)/\sin\theta_0$, and a completely random distribution (3D powder sample) $f(\theta,\phi) = 1/(4\pi)$. The real distribution is generally somewhere between these limits. A non-random orientational distribution can be induced in several ways, for example, by a magnetic field, by interactions at the sample boundaries, or by hydrodynamic shearing. In most cases, however, the spectral parameters $\langle\chi\rangle$ and η can be obtained with sufficient accuracy directly from the singular features of the lineshape. The lineshape from a uniaxial phase has potential singularities at $\omega = \pm\omega_Q(\theta = 0°)$ and at $\omega = \mp\omega_Q(\theta = 90°)$. For a biaxial phase, there are three pairs of potential singularities at $\omega = \pm\omega_Q(\theta = 0°)$, at $\omega = \mp\omega_Q(\theta = 90°,\ \phi = 0°)$, and at $\omega = \mp\omega_Q(\theta = 90°, \phi = 90°)$. These singularities are smoothed out by homogeneous broadening due to transverse relaxation. For particular orientational distributions $f(\theta,\phi)$, some of the singularities may completely disappear. For 3D powder samples, for example, the $\theta = 0°$ singularities and, in the biaxial case, also the $(\theta = 90°, \phi = 90°)$ singularities may produce sharp 'shoulders' but do not give rise to peaks.

3.2. *Hexagonal phase*

Figure 2 shows the lineshapes obtained from the two samples in the H_α phase at 35°C and in the R_α phase at 25°C. The R_α lineshapes were virtually the same at 25°C and 30°C, while the H_α lineshapes showed only a small decrease of the line splitting with increasing temperature in the range 35–50°.

Apart from the sharp $\theta = 90°$ peaks at $\pm 5{\cdot}8$ kHz and the associated $\theta = 0°$ shoulders at $\pm 11{\cdot}6$ kHz, the H_α spectrum of sample **S** displays a second spectral component with powder-like peaks at $\pm 9{\cdot}7$ kHz and shoulders at $\pm 19{\cdot}3$ kHz. We ascribe this second component to a small amount of L_α phase in equilibrium with H_α [19]. The relative intensity of the second component does not change significantly with temperature. It is present also in the H_α spectra of sample D, although not so clearly visible, since the $\theta = 90°$ peaks of the second component almost

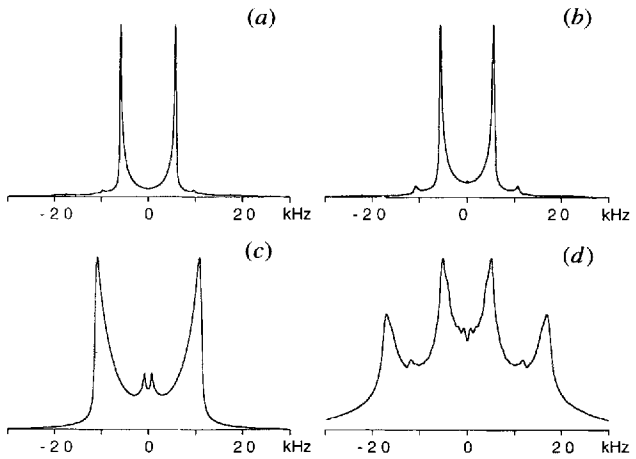

Figure 2. ^{2}H NMR spectra from sample **S** (α-^{2}H SdS) at (*a*) 35°C and (*c*) 25°C, and from sample **D** (α-^{2}H decanol) at (*b*) 35°C and (*d*) 25°C. The frequency axis defines the base line of the symmetrized spectra.

coincide with the $\theta = 0°$ shoulders from the H_α phase. As the second component does not significantly affect the spectral analysis, it will henceforth be ignored.

According to equation (2), the $\omega = \mp \omega_Q(\theta = 90°)$ singularities in the spectra from the uniaxial ($\eta = 0$) H_α phase correspond to a quadrupole splitting (in Hz)

$$\Delta\nu_Q(\theta = 90°) = \tfrac{3}{4}\langle\chi\rangle. \qquad (5)$$

From the peak-to-peak separation in the spectrum (see figure 2 (*a*)), we thus obtain $\langle\chi\rangle = 15{\cdot}47$ kHz. A complete lineshape fit, shown in figure 3 (*a*), with a gaussian distribution function $f(\theta)$, yields a marginally larger QCC: $\langle\chi\rangle = 15{\cdot}69 \pm 0{\cdot}05$ kHz. The orientational distribution is

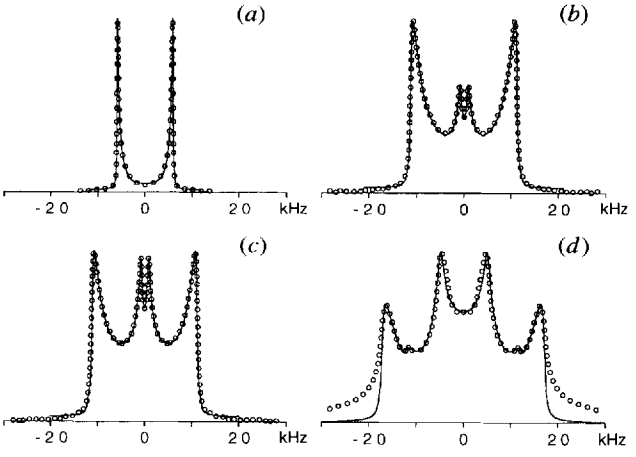

Figure 3. Experimental (circles) and simulated (solid line) ^{2}H NMR spectra of (*a*) sample **S** at 35°C (H_α phase); (*b*) sample **S** at 30°C (R_α phase); (*c*) sample **S** at 30°C (R_α phase) after thermal treatment (cf. text), and (*d*) sample **D** at 30°C (R_α phase).

peaked at $\theta_0 = 90°$ with a root-mean-square angular spread of *c.* 15°. Since the largest principal EFG component $\langle V_{zz}^C\rangle$ in the uniaxial H_α phase is along the axis of the cylindrical surfactant aggregates, we can conclude that the aggregates *spontaneously* orient (preferentially) perpendicular to the axis of the sample tube (which is parallel to the magnetic field [21]).

The QCC values obtained as described above from the two samples in the H_α phase in the temperature range 35–50°C are collected in table 1. From these values we may calculate the second-rank orientational order parameter S for the C–^{2}H bonds in the α-methylene groups of SdS and decanol as $S = 2\langle\chi\rangle/\chi$, with the C–^{2}H QCC $\chi = 170$ kHz. We thus obtain $S = 0{\cdot}182$–$0{\cdot}184$ for SdS and $S = 0{\cdot}169$–$0{\cdot}178$ for decanol. These values are in the expected range [22, 23].

3.3. *Rectangular phase*

The spectrum from sample **S** in the R_α phase exhibits two pairs of peaks (see figure 2 (*c*)). Since we know from the analysis of the H_α lineshape that the aggregates are predominantly oriented perpendicular to the magnetic field, we ascribe these peaks to the two pairs of $\theta = 90°$ singularities in a biaxial spectrum (cf. above). According to equation (2) the two line splittings are then given approximately by

$$\Delta\nu_Q(\theta = 90°, \phi = 0°) = \tfrac{3}{4}(1 - \eta)\langle\chi\rangle, \qquad (6a)$$

and

$$\Delta\nu_Q(\theta = 90°, \phi = 90°) = \tfrac{3}{4}(1 + \eta)\langle\chi\rangle. \qquad (6b)$$

From the spectrum in figure 2 (*c*) we thus obtain $\langle\chi\rangle = 15{\cdot}4$ kHz and $\eta = 0{\cdot}87$ at 25°C. A lineshape analysis, shown in figure 3 (*b*) (for 30°C), with a suitably parameterized distribution function $f(\theta, \phi)$, refined these estimates to $\langle\chi\rangle = 16{\cdot}0 \pm 0{\cdot}2$ kHz and $\eta = 0{\cdot}85 \pm 0{\cdot}02$ (at 25°C). The lineshape analysis again gave a root-mean-square spread in θ of *c.* 15° around the preferred orientation $\theta_0 = 90°$. Furthermore, a non-random (but broad) distribution of the azimuthal angle ϕ was also required to reproduce the lineshape [24].

The relative intensity of the two pairs of peaks in the R_α spectrum of sample **S** was found to depend on the thermal history of the sample. The spectrum in figure 3 (*b*) was obtained from a sample which had not been exposed to higher temperatures than 30°C. Raising the temperature to 40°C (in the H_α phase) for 30 min. and then returning to 30°C we obtained (after thermal equilibration) the spectrum shown in figure 3 (*c*). A lineshape analysis showed that the enhanced intensity of the central peaks is due to a broader θ distribution. The deduced values for $\langle\chi\rangle$ and η did not change, however, indicating that the microstructure was not affected.

The spectrum from sample **D** in the R_α phase (see figure 2 (*d*) is qualitatively different from that obtained from

Table 1. Parameters derived from lineshapes.

Sample	Temperature/°C	Phase	$\langle\chi\rangle$/kHz	η	θ_0/degree
S	25	R_α	16·1 ± 0·2	0·86 ± 0·02	90
S	30	R_α	16·0 ± 0·2	0·85 ± 0·02	90
S	35	H_α	15·69 ± 0·05	0	90
S	40	H_α	15·67 ± 0·05	0	90
S	45	H_α	15·55 ± 0·05	0	90
S	50	H_α	15·47 ± 0·05	0	90
D	25	R_α	23·0 ± 0·3	0·39 ± 0·02	0
D	30	R_α	22·4 ± 0·3	0·41 ± 0·02	0
D	35	H_α	15·1 ± 0·1	0	90
D	40	H_α	14·9 ± 0·1	0	90
D	45	H_α	14·5 ± 0·1	0	90
D	50	H_α	14·4 ± 0·1	0	90

sample **S** (see figure 2(*c*)). In particular, three pairs of singularities are now evident. In accordance with the previous discussion, we identify the outermost peaks with the $\theta = 0°$ singularities, with the splitting

$$\Delta\nu_Q(\theta = 0°) = \tfrac{3}{2}\langle\chi\rangle. \tag{7}$$

The other two splittings are given by equations (6), which give $\langle\chi\rangle = 22{\cdot}6$ kHz and $\eta = 0{\cdot}40$. The outer splitting yields with equation (7) the same $\langle\chi\rangle$ value, thus confirming the assignment of the peaks. A lineshape analysis, shown in figure 3(*d*) (for 30°C), refined these estimates to $\langle\chi\rangle = 23{\cdot}0 \pm 0{\cdot}3$ kHz and $\eta = 0{\cdot}39 \pm 0{\cdot}02$ (at 25°C).

The distribution function $f(\theta, \phi)$ required to reproduce the lineshape differs qualitatively from that found from the R_α lineshape of sample **S**. In particular, the θ distribution is now peaked at $\theta_0 = 0°$ (and is somewhat broader) rather than at $\theta_0 = 90°$ (as in the R_α phase of sample **S** and in the H_α phase of *both* samples). Since the aggregate orientation cannot change when sample **D** is brought (by a slight increase of temperature) from the R_α phase to the H_α phase, we conclude that the largest principal EFG component $\langle V_{zz}^C\rangle$ is no longer along the aggregate axis in the R_α phase of sample **D**. It has previously been shown [8–12] that as the aggregate cross-section is deformed from a circular shape, at a certain point the orientation of the axis associated with largest EFG component changes by 90° from being parallel to the C_2 axis of the phase to being parallel to the shorter side of the rectangular unit cell. These two regimes are referred to as the small deformation regime (SDR) and the large deformation regime (LDR). We thus conclude that the SdS spectra (sample **S**) from the R_α phase are in the SDR, while the decanol spectra (sample **D**) from the R_α phase are in the LDR. This conclusion is supported by the large QCC values (see table 1) obtained from sample **D** in the R_α phase (cf. § 4).

Since the two samples have identical composition (on a molar basis), the surfactant aggregates should have the same structure in the two samples. The finding that the samples are in different spectral regimes therefore implies that *the SdS and decanol molecules are non-uniformly distributed over the aggregate cross-section.* In fact, the qualitative difference between the SdS and decanol spectra in figures 2(*c*) and (*d*) constitutes direct evidence for such molecular segregation. *Qualitative* evidence of molecular segregation in the R_α phase of the present system has previously been obtained from neutron scattering [5]. In the following section, we use a geometric model to characterize *quantitatively* the extent of molecular segregation as well as the aggregate shape. Since the parameters $\langle\chi\rangle$ and η are virtually independent of temperature in the R_α phase (see table 1), we henceforth consider only the 30°C data.

4. Microstructure in the R_α phase

4.1. *Motional averaging of the quadrupole coupling in the R_α phase*

In order to extract information about the microstructure from the parameters $\langle\chi\rangle$ and η derived from the lineshape, it is convenient to transform the motionally averaged EFG components $\langle V_{\alpha\alpha}^C\rangle$ to the principal frame F of the instantaneous C–^{2}H EFG tensor via two intermediate frames, R and N. The ribbon frame R is fixed in the surfactant aggregate and differs from the crystal frame C (fixed in the unit cell) only if the unit cell contains aggregates with differently oriented cross-sections, as for an R_α phase of plane group pgg. The local interface frame N defines the preferred orientation of surfactant molecules with respect to the aggregate surface. In the geometrical model to be considered, the z_N axis coincides with the local normal to the aggregate surface.

Performing the rotational transformations as in [12] and making the (excellent) approximations of uniaxiality in the F and N frames, we obtain

$$\langle\chi\rangle = \tfrac{1}{2}[3\langle S\cos^2\theta_{RN}\rangle - \langle S\rangle]\chi, \tag{8}$$

and

$$\eta = B\frac{\langle S\sin^2\theta_{RN}\cos 2\phi_R\rangle}{\langle S\cos^2\theta_{RN}\rangle - \frac{1}{3}\langle S\rangle}. \quad (9)$$

The orientation of the local surface normal with respect to the R frame is specified by the polar (θ_{RN}) and azimuthal (ϕ_R) angles. The factor B allows for the possibility of non-equivalent aggregates in the unit cell. For plane group cmm, $B = 1$, while for plane group pgg, $B = \cos(2\alpha)$, with α the tilt angle of the aggregate cross-section with respect to the unit cell axes. In the R_α (pgg) phase of the present system $2\alpha \leqslant 15°$ [7], whence $0{\cdot}97 \leqslant B \leqslant 1$. We can therefore set $B = 1$ for both plane groups. Finally, $S = \langle P_2(\cos\theta_{NF})\rangle$ is the second-rank orientational order parameter for the α-methylene C–^{2}H bond with respect to the local surface normal. Since the interface curvature and head group areas vary along the perimeter of the aggregate cross-section, we allow for a spatial variation in S.

In the small-deformation regime (SDR), where the z_R axis is oriented along the length of the aggregate, we have $\theta_{RN} = 90°$, whence

$$\langle\chi\rangle = -\tfrac{1}{2}\langle S\rangle\chi, \quad (10)$$

and

$$\eta = -3\frac{\langle S\cos 2\phi_R\rangle}{\langle S\rangle}. \quad (11)$$

In the large-deformation regime (LDR), where the z_R axis is perpendicular to the least curved part of the aggregate cross-section, we have $\phi_R = 0°$, whence

$$\eta = \frac{\chi\langle S\rangle}{\langle\chi\rangle} - 1. \quad (12)$$

In the H_α phase, with aggregates of circular cross-section, we have $\theta_{RN} = 90°$, $f(\phi_R) = 1/(2\pi)$, and uniform S, whence

$$\langle\chi\rangle = -\tfrac{1}{2}S\chi, \quad (13)$$

and

$$\eta = 0 \quad (14)$$

Introducing the ratio of the magnitudes of the residual QCCs in the R_α and H_α phases (at the same temperature),

$$Q = \left|\frac{\langle\chi\rangle_{R_\alpha}}{\langle\chi\rangle_{H_\alpha}}\right|, \quad (15)$$

we obtain

$$\frac{\langle S\rangle_{R_\alpha}}{S_{H_\alpha}} = Q \quad \text{(SDR)}, \quad (16a)$$

and

$$\frac{\langle S\rangle_{R_\alpha}}{S_{H_\alpha}} = \tfrac{1}{2}(1+\eta)Q \quad \text{(LDR)}. \quad (16b)$$

We can thus obtain a measure of the spatial variation of the order parameter without invoking a model for the aggregate geometry. Making a small linear extrapolation of the H_α QCCs in table 1 to 30°C, we obtain for SdS $Q_S = 1{\cdot}01 \pm 0{\cdot}01$ and for decanol $Q_D = 1{\cdot}46 \pm 0{\cdot}02$. Since the SdS spectra are in the SDR and the decanol spectra are in the LDR (cf. § 3.3), we obtain from equations (16) $\langle S\rangle_{R_\alpha}/S_{H_\alpha} = 1{\cdot}01 \pm 0{\cdot}01$ for SdS and $\langle S\rangle_{R_\alpha}/S_{H_\alpha} = 1{\cdot}03 \pm 0{\cdot}05$ for decanol. The spatially averaged order parameter in the biaxial aggregates of the R_α phase is thus not significantly different from the order parameter in the circular-cylindrical aggregates of the H_α phase.

4.2. *The ribbon model*

In order to separate the effects on $\langle\chi\rangle$ and η of the shape of the aggregate cross-section, of the molecular distribution within the aggregate, and of a spatially varying order parameter, we must specify a model for the aggregate geometry. Three such models have been proposed. In the ribbon model [8–11], the aggregate comprises a central lamellar region flanked by two hemi-cylindrical edges. In the hexagonal rod model [16], the aggregate cross-section has the shape of an asymmetric hexagon. While these two models have the virtue of mathematical simplicity, they have certain unphysical features: sharp edges in the hexagonal rod and a discontinuous curvature in the ribbon. These unphysical features are not present in the elliptic rod model [12], which also permits an analytical treatment. For the small departures from circular cross-section (an aspect ratio of 1·5 is typical [18]) so far deduced in R_α phases, the elliptic rod model probably gives the most faithful representation of the aggregate shape. For the purpose of analysing molecular segregation in two-component aggregates, however, the elliptic rod model requires further assumptions to be made about the packing of the surfactant tails. In the following, we shall therefore use the ribbon model, which requires no further assumptions.

In its most general form [10, 11], the ribbon model relates the four experimental quantities, Q and η for SdS (**S**) and decanol (**D**), to four model parameters: the fraction W of each molecular species residing in the lamellar region (cf. figure 4) and the ratio $\mu = S_L/S_C$ of the order parameters in the two regions for each molecular species. With SdS in the SDR and decanol in the LDR we obtain from equations (8)–(15), assuming $S_C = S_{H\alpha}$,

$$W_S = 1 - \left(1 - \frac{\eta_S}{3}\right)Q_S, \quad (17a)$$

$$W_D = 1 - \tfrac{2}{3}\eta_D Q_D, \quad (17b)$$

$$\mu_S = \left[1 - \frac{3}{\eta_S}\left(1 - \frac{1}{Q_S}\right)\right]^{-1}, \quad (17c)$$

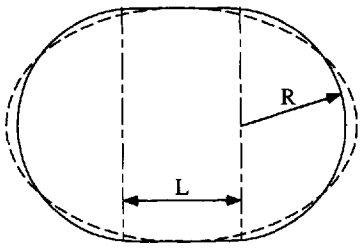

Figure 4. Aggregate cross-section in the ribbon model with aspect ratio $\rho = (L + 2R)/(2R) = 1{\cdot}39$. For comparison, we show an elliptic cross-section ($\rho = 1{\cdot}50$) with the same area and the same minor axis.

and

$$\mu_D = \frac{1}{4}\left[1 - \left(1 - \frac{1}{2Q_D}\right)\left(1 - \frac{\eta_D}{3}\right)^{-1}\right]^{-1}. \qquad (17d)$$

The results obtained from equation (17) for the present R_α sample (at 30°C) are collected in table 2. As expected [25], the order parameter appears to be slightly higher in the lamellar part of the ribbon than in the hemi-cylindrical part (or in the H_α phase). The fraction W of molecules residing in the lamellar part is twice as large for decanol as for SdS, implying a highly non-uniform molecular distribution (cf. below).

The quantities W_S and W_D depend on the cross-sectional aspect ratio ρ (cf. figure 4) as well as on the extent of molecular segregation. The latter can be quantified in terms of the local mol fractions x_L and x_C of the two components, obtained from W_S, W_D and the known overall SdS/decanol mol ratio $z = 4{\cdot}70$ as [11]

$$x_L^D = 1 - x_L^S = \left(1 + z\frac{W_S}{W_D}\right)^{-1}, \qquad (18a)$$

and

$$x_C^D = 1 - x_C^S = \left(1 + z\frac{1 - W_S}{1 - W_D}\right)^{-1}, \qquad (18b)$$

The results, given in table 2, should be compared with the overall mol fractions: $x_S = 0{\cdot}825$ and $x_D = 0{\cdot}175$. As expected, the local mol fractions differ most for the least abundant component: the decanol concentration is more than three times as high in the lamellar part as in the hemi-cylindrical parts.

Table 2. Microstructural parameters for the R_α phase at 30°C calculated with the ribbon model.

Property	SdS	Decanol
$\lvert\langle\chi\rangle_{R\alpha}/\langle\chi\rangle_{H\alpha}\rvert$†	1·01 ± 0·01	1·46 ± 0·02
$\langle S\rangle_{R\alpha}/S_{H\alpha}$†	1·01 ± 0·01	1·03 ± 0·05
S_L/S_C	1·04 ± 0·04	1·05 ± 0·04
W	0·28 ± 0·01	0·60 ± 0·02
x_L	0·68 ± 0·01	0·32 ± 0·01
x_C	0·90 ± 0·01	0·10 ± 0·01
σ_L/σ_C	1·53 ± 0·03	
ρ	1·39 ± 0·01	

† Model-independent quantities.

Since SdS and decanol have the same C_{10} alkyl chain, simple geometrical considerations yield for the cross-sectional aspect ratio

$$\rho = 1 + \frac{\pi}{4}\frac{W_D + zW_S}{(1 - W_D) + z(1 - W_S)}. \qquad (19)$$

With W_S and W_D from table 2 we thus obtain $\rho = 1{\cdot}39 \pm 0{\cdot}01$.

5. Discussion

5.1. *Aggregate shape*

Given the assumed ribbon-like aggregate geometry, we obtain an aspect ratio of $\rho = 1{\cdot}39 \pm 0{\cdot}01$ for the cross-section of the paraffinic core of the aggregates. This represents a rather modest deviation from the circular-cylindrical aggregates in the H_α phase. Taking $R = 13{\cdot}5$ Å, which is slightly smaller than the all-*trans* decyl chain length (14·2 Å) and slightly larger than the core radius (13·2 Å) in the decanol-free H_α phase [7], we obtain a cross-sectional area of 856 Å^2, in excellent agreement with the area obtained from X-ray scattering [7]. Our aspect ratio, however, is substantially smaller than the value $\rho = 2{\cdot}7$ inferred from X-ray data [4, 6] (where it was assumed that $2R$ equals the bilayer thickness in the L_α phase), and also significantly smaller than the value $\rho = 1{\cdot}76$ (unknown accuracy) deduced [6] from neutron scattering data from an R_α (pgg) sample at 23°C with molar ratios SdS/decanol and H_2O/SdS of 4·46 and 14·9 (we have 4·70 and 13·0). Since the aspect ratio is relatively small, any errors introduced in the data analysis by forcing the aggregates to adopt a ribbon-like geometry should be unimportant. This point is illustrated in figure 4, showing an elliptic cross-section with the same area and the same minor axis as for the ribbon geometry.

In analysing our data we have tacitly assumed that the H_α phase has a classical microstructure with cylinders of circular cross-section. On the basis of X-ray and neutron scattering data, however, it has been suggested that, at the decanol content of our samples, the aggregates are ribbon-like (with orientationally disordered cross-sections) already in the H_α phase [6, 26]. In particular, neutron scattering data were taken as evidence for molecular segregation, implying a non-circular aggregate cross-section in the H_α phase [26]. In a recent publication from the same group, however, the concept of a deformed aggregate section in the H_α phase appears to have been abandoned [7].

Our NMR data are fully consistent with a classical microstructure in the H_α phase. According to table 1 the residual QCC $\langle\chi\rangle$ is only *c.* 5 per cent smaller for decanol than for SdS (in the H_α phase), as expected from the order parameter S for decanol and SdS [22, 23]. If the cross-sectional shape and molecular distribution in the H_α phase were such that, for decanol, the largest principal EFG component *in the ribbon-fixed R frame* was perpendicular to the long axis of the aggregate (as in the R_α phase), then the orientational disorder would reduce $\langle\chi\rangle$ by a factor 2 for decanol, as compared to SdS (since the order parameter S is essentially invariant to external conditions such as interfacial curvature [22, 23]). This is *not* observed (cf. table 1). According to equation (17), the largest aspect ratio consistent with the observed near equality of $\langle\chi\rangle$ for SdS and decanol in the H_α phase is $\rho = 1 + \pi x_C/(8\mu x_L)$. Using the decanol data from table 2, we thus obtain an upper limit of $\rho = 1{\cdot}12$ for the aggregates in the H_α phase.

As seen from table 1, the temperature dependence of $\langle\chi\rangle$ and η in the R_α phase is hardly significant, while that of $\langle\chi\rangle$ in the H_α phase is weak and linear. These observations suggest an essentially invariant aggregate shape within either phase, with a sudden, symmetry-breaking, shape transformation at the H_α–R_α transition. In particular, it does not appear that the H_α–R_α transition is induced by a continuous anisotropic growth of the aggregate cross-section [6].

Our result, $\rho = 1{\cdot}4$, for the aspect ratio of the aggregates in the investigated R_α samples falls squarely within the range deduced for R_α phases in a variety of binary systems [13, 18]. In one system, cesium tetradecanoate/D_2O, the R_α–H_α transition was reported to be of second order [13]. This conclusion was based on the apparent absence of a two-phase region and was consistent with the gradual change of the aspect ratio (as deduced from the D_2O splitting) from 1·5 to 1 as the H_α phase was approached [13]. In the present system, however, the R_α–H_α and R_α–L_α transitions are both of first order, as is evident from the intervening polyphasic regions in figure 1.

5.2. *Molecular segregation*

As seen from table 2, the distribution of SdS and decanol within the aggregate is highly non-uniform; the SdS molecules prefer the hemi-cylindrical edges (by a factor 1·3), while the decanol molecules prefer the central lamellar region (by a factor 3·2). Previously, molecular segregation in the aggregates of the present R_α phase has been inferred from neutron scattering data [5]; however, the extent of segregation was not quantified. In fact, the scattering study did not identify the nature of the segregation (decanol accumulation in the flat region and SdS accumulation in the curved region, or vice versa): this was only inferred by analogy with the phase progression induced by varying the decanol/SdS ratio.

When the circular symmetry of the aggregate cross-section is broken (presumably at the phase transition), the system acquires a new degree of freedom (a variable local surfactant concentration), which has the effect of stabilizing the R_α phase. Molecular segregation is opposed by the reduced entropy of mixing within the aggregate. Assuming ideal mixing, the resulting free energy increase per surfactant molecule is

$$\Delta g_{\text{mix}} = k_B T \sum_\alpha x_\alpha \left[W_\alpha \ln \frac{x_L^\alpha}{x_\alpha} + (1 - W_\alpha) \ln \frac{x_C^\alpha}{x_\alpha} \right], \quad (20)$$

where the sum runs over the two components. With data from table 2 we thus obtain $\Delta g_{\text{mix}} = 0{\cdot}031 k_B T$. This modest free energy price must be more than compensated by a more favourable water-head group interaction in the curved regions (where the head group area is larger) and by more favourable electrostatic interactions within and between the aggregates.

At a mean-field level of approximation, the electrostatic effects of molecular segregation may be treated in terms

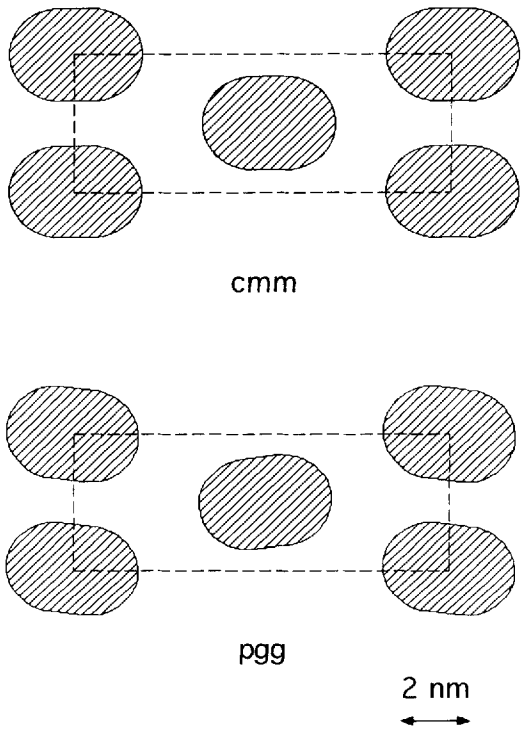

Figure 5. Unit cells for the two possible lattice symmetries of the investigated R_α phase. The cross-sections shown correspond to the paraffinic aggregate core (excluding head groups and counterions) with aspect ratio $\rho = 1{\cdot}39$ as determined here. The aggregate volume fraction ($\phi_{\text{core}} = 0{\cdot}432$) corresponds to samples **S** and **D**. The smallest lattice parameter (38 Å) and the tilt angle in the pgg phase ($2\alpha = 15°$) are taken from previous scattering studies [6, 7].

of the inhomogeneous surface charge density σ. The ratio of the surface charge densities in the cylindrical and lamellar regions (assumed homogeneous) is obtained from geometrical considerations as

$$\frac{\sigma_C}{\sigma_L} = \frac{1}{2}\frac{z + W_D/W_S}{z + (1 - W_D)/(1 - W_S)}. \quad (21)$$

With data from table 2, we thus obtain $\sigma_C/\sigma_L = 0{\cdot}67 \pm 0{\cdot}02$, to be compared with $\sigma_C/\sigma_L = 0{\cdot}50$ in the absence of molecular segregation. The segregation-induced enhancement of the charge density at the curved edges has two effects. First, it lowers the free energy of the aggregate by reducing the electric field penetrating into the non-polar hydrocarbon core [27]. Secondly, it enhances the (two-dimensional) electric quadrupole moment of the aggregate (including its counterions) [5] and, hence, affects the interaction between adjacent aggregates.

The importance of inter-aggregate interactions can be appreciated from figure 5, showing the cross-sections of the paraffinic aggregate cores on rectangular lattices, with the smallest lattice parameter taken as 38 Å [7] and the largest lattice parameter determined by the composition. The inter-aggregate interactions evidently cause the aggregates to pack non-uniformly, with the flat interfaces closely spaced. Assuming that $R = 13{\cdot}5$ Å (cf. above) and that the sulphate head groups protrude 3 Å out from the core, the head groups of adjacent aggregates are separated by merely 5 Å. The electrostatic repulsion between head groups on adjacent interfaces must clearly be an important driving force for molecular segregation within the aggregates. Furthermore, at such small separations, the effect of the mean quadrupole moment of the aggregate is probably overwhelmed by ionic and steric correlation effects. This should be a general feature of R_α phases, which usually occur at higher volume fractions [18] than the present one.

We are grateful to Dr Lars A. Bengtsson for assistance with the Varian spectrometer, and the Swedish Research Council for Engineering Sciences and the Swedish Natural Science Research Council for financial support.

References

[1] LUZZATI, V., MUSTACCHI, H., SKOULIOS, A., and HUSSON, F., 1960, *Acta crystallogr.*, **13,** 660.
[2] HUSSON, F., MUSTACCHI, H., and LUZZATI, V., 1960, *Acta crystallogr.*, **13,** 668.
[3] TIDDY, G. J. T., 1980, *Phys. Rep.*, **57,** 1.
[4] HENDRIKX, Y., and CHARVOLIN, J., 1981, *J. Phys., Paris*, **42,** 1427.
[5] ALPÉRINE, S., HENDRIKX, Y., and CHARVOLIN, J., 1985, *J. Phys. Lett., Paris*, **46,** 27.
[6] HENDRIKX, Y., and CHARVOLIN, J., 1992, *Liq. Crystals*, **11,** 677.
[7] CHARVOLIN, J., 1993, *Liq. Crystals*, **13,** 829.
[8] CHIDICHIMO, G., VAZ, N. A. P., YANIV, Z., and DOANE, J. W., 1982, *Phys. Rev. Lett.*, **49,** 1950.
[9] CHIDICHIMO, G., GOLEMME, A., DOANE, J. W., and WESTERMAN, P. W., 1985, *J. chem. Phys.*, **82,** 536.
[10] CHIDICHIMO, G., GOLEMME, A., and DOANE, J. W., 1985, *J. chem. Phys.*, **82,** 4369.
[11] POPE, J. M., and DOANE, J. W., 1987, *J. chem. Phys.*, **87,** 3201.
[12] QUIST, P.-O., and HALLE, B., 1988, *Molec. Phys.*, **65,** 547.
[13] BLACKBURN, J. C., and KILPATRICK, P. K., 1992, *J. Coll. Interf. Sci.*, **149,** 450.
[14] BLACKBURN, J. C., and KILPATRICK, P. K., 1992, *Langmuir*, **8,** 1679.
[15] BLACKBURN, J. C., and KILPATRICK, P. K., 1993, *J. Coll. Interf. Sci.*, **157,** 88.
[16] HENRIKSSON, U., BLACKMORE, E. S., TIDDY, G. J. T., and SÖDERMAN, O., 1992, *J. phys. Chem.*, **96,** 3894.
[17] KANG, C., SÖDERMAN, O., ERIKSSON, P. O., and STAEL VON HOLSTEIN, J., 1992, *Liq. Crystals*, **12,** 71.
[18] HAGSLÄTT, H., SÖDERMAN, O., and JÖSSON, B., 1992, *Liq. Crystals*, **12,** 667.
[19] The ratio of the L_α to H_α splittings is 1·65, i.e. smaller than the ideal factor 2. This presumably reflects structural defects in the L_α phase at this low decanol content [20].
[20] HENDRIKX, Y., CHARVOLIN, J., KÉKICHEFF, P., and ROTH, M., 1987, *Liq. Crystals*, **2,** 677.
[21] The highly viscous H_α and R_α phases are not significantly aligned by the magnetic field. Magnetic alignment of the H_α phase can be achieved, however, by first heating the sample to the isotropic solution phase.
[22] SEELIG, J., and NIEDERBERGER, W., 1974, *Biochemistry*, **13,** 1585.
[23] QUIST, P.-O., FONTELL, K., and HALLE, B., 1994, *Liq. Crystals*, **16,** 235.
[24] The presence of a non-uniform ϕ distribution was confirmed by investigating the orientation dependence of the lineshape in a probe configuration with the magnetic field perpendicular to the tube axis. These experiments also revealed a non-uniform distribution of the aggregate axis in the plane normal to the tube axis.
[25] CHARVOLIN, J., and HENDRIKX, Y., 1985, *Nuclear Magnetic Resonance of Liquid Crystals*, edited by J. W. Emsley (D. Reidel Publ. Co.), p. 449.
[26] HENDRIKX, Y., and CHARVOLIN, J., 1988, *Liq. Crystals*, **3,** 265.
[27] HALLE, B., LANDGREN, M., and JÖNSSON, B., 1988, *J. Phys., Paris*, **49,** 1235.